Hardware in the Loop-Based Testing of Three Schemes for Mitigation the Effect of Unsymmetrical Grid Faults on DFIG

ESSAMUDIN ALI EBRAHIM, MAGED N. F. NASHED, MONA N. ESKANDER
Power Electronics and Energy Conversion Department,
Electronics Research Institute,
Joseph Tito St., Huckstep, Qism El-Nozha, Cairo Governorate, Cairo,
EGYPT

Abstract: - This paper presents three-proposed schemes to mitigate the effect of unsymmetrical voltage sag fault on a wind-driven grid-connected Double Fed Induction Generator (DFIG). The first tested scheme comprises a static compensator (STATCOM) connected to the DFIG stator, while a three-phase parallel RL external impedance is connected to the rotor circuit in the second scheme. The STATCOM and the added rotor impedance are connected simultaneously in the third scheme. The effect of applying the three schemes on the responses of the stator and rotor voltages and currents, the dc-link voltage and current, the electrical torque, and the rotor speed during an unsymmetrical voltage sag are presented and compared at sub-and super-synchronous speeds. All systems were emulated, implemented, and tested through an OPAL RT-4510 Digital Real-Time Simulator (DRTS) in a Hardware-In-the-Loop (HIL) application. The internal Field-Programmable Gate Array (FPGA) chip assisted in using this platform as a Rapid Control Prototyping (RCP) for virtual mitigation control and testing. The Matlab/ Simulink RT-lab software packages combination helped in the RT development environment. All real-time waveforms of parameters for the proposed scenarios were monitored through the HIL-controller and data acquisition interface and then compared with the simulated results. The results reveal that the simulation waveforms and the real time waveforms are congruent. Results prove the better performance of the DFIG during unsymmetrical voltage sag for sub-synchronous speed when applying both protection schemes, while best results are obtained when using only the rotor impedance at super-synchronous speed operation of the DFIG.

Key-Words: - Double Fed Induction Generator (DFIG), Hardware In the loop (HIL), Rapid Control Prototyping (RCP), Static Compensator (STATCOM), Unsymmetrical grid fault, Voltage sag, Wind Energy

Received: September 9, 2022. Revised: August 29, 2023. Accepted: September 27, 2023. Published: October 30, 2023.

1 Introduction

The double-fed induction generator (DFIG) is employed in variable speed wind energy conversion systems (WECS), where the DFIG stator is directly connected to the grid, and its rotor is connected to the grid via two back-to-back converters and a transformer. The DFIG has a large share in the wind energy conversion systems market due to its benefits of variable speed operation, lower cost rotor converters, and active and reactive power independent control, [1]. However, its low voltage ride-through (LVRT) capability is due to its stator's direct connection to the grid, [2]. Several researches were done to solve the problems associated with symmetrical grid faults, [3].

The unsymmetrical grid faults lead to high electric torque pulsations, which adversely affect the wind turbine and the associated mechanical components such as the gearbox and bearings, [4]. These faults also cause high DC link voltage ripples, which shorten the lifetime of the DC link capacitor, and lead to high rotor current transients which damage the rotor converter. Reference, [5], proposed various techniques to mitigate the effect of unsymmetrical grid faults on the performance of grid-connected DFIG. The authors compared the effects of both abrupt and discrete grid voltage sags on the doubly-fed induction generator performance without proposing a solution for mitigating these effects.

In, [6], the authors proposed a control strategy for both the rotor side and the grid side converters of a DFIG-based wind turbine system to enhance the low voltage ride through non-ideal proportional resonant (PR) controllers for both converters to limit rotor current surges and to keep the dc-link voltage nearly constant during the grid faults. However, sharp peaks were still obvious in DC voltage.

A gate-controlled series capacitor (GCSC) was proposed in, [7], to be inserted in series with the generator rotor as soon as a voltage dip occurs, increasing the voltage seen by the rotor winding and consequently, limiting the rotor over-current and protecting the rotor side inverter. This method ignored the effect of the faults on the stator windings.

In, [8], an inductance emulating control design was proposed for the FRT of a DFIG-based wind turbine. A feed-forward current reference control was proposed in, [9], to improve the transient performance of a DFIG-based wind turbine during grid faults. A DVR was proposed in, [10], to compensate for voltage sags, which have better performance during symmetrical faults. Sliding mode control was proposed in, [11], by applying an infinite-frequency switching control to keep output, the sliding variable, at zero. Such high-frequency control switching generates undesirable system vibrations. A combination of series-dynamic-resistors and stator-side-fault-current limiters were proposed in, [12], and a STATCOM-based approach was proposed in, [13]. However, those designs cannot ensure the dynamic stability of the system during grid faults. A multi-target control strategy for DFIG using a virtual synchronous generator (VSG) under unbalanced grid voltage is proposed in, [14] by introducing the extended power method and resonant controller into the conventional VSG. Electric torque variations were still present in the presented results. In, [15], the authors focused on control strategies to reduce the harmonics generated in the DFIG- wind turbine system due to unsymmetrical grid fault. The current and voltage peaks were not considered.

The authors in, [16], proposed a modified dynamic model of the DFIG subjected to symmetrical and unsymmetrical fault. The results showed lower oscillations during the three-phase fault (symmetrical fault), but large oscillations with relatively small duration, occurred during the unsymmetrical grid fault. The authors in, [17] proposed a modified DVR topology to regulate the stator voltage through the rotor power converters to improve fault-ride-through of grid-connected DFIG-WECS.

A saturated-core fault-current-limiter that is based on the change in the permeability between the saturated and unsaturated conditions has been presented in, [18]. The occurrence of unsymmetrical grid fault, results in a negative sequence voltage component that generates a second-order voltage harmonic interference in the *d–q* transformation of the grid voltage. Thus a low-pass filter was proposed and applied for the determination of the *q*-axis component of the grid voltage, according to, [19].

Series compensated grid-connected topology for the DFIG is used for minor voltage sags and unbalanced and distorted grid disturbances, [20], [21], [22]. The performance during symmetrical and unsymmetrical faults is observed in, [23]. Rotor current limitation during the fault, using a rotor-side converter control scheme, improved the performance of the DFIG in, [24]. However, an increase in the rotor speed and oscillations are observed in the power and electromagnetic torque.

A common- STATCOM topology with a PQ-based control strategy is proposed in, [25], where a common capacitor between the rotor-side converter and the grid-side converter is shared by the STATCOM. In, [26], the voltage dips and voltage harmonics were compensated via a modified DVR topology in WECS-DFIG system.

The paper is focused on symmetrical faults, while a short study was presented for unsymmetrical voltage sag, hence the effect of DVR was not clear.

In, [27], the authors proposed an enhanced dynamic voltage restorer (EDVR) to improve the voltage stability of a microgrid. In, [28], the authors proposed a fault ride through scheme for DFIG-based wind energy systems combining the properties of fractional order sliding mode control with the active/reactive power control capability of the dynamic voltage restorer, and the high-power density of superconducting magnetic material. This system requires complex control strategy and high cost. A control strategy based on super-capacitors was proposed for simultaneous consideration of voltage ride through and frequency regulation under power grid faults, [29].

In this paper, three control schemes are proposed to mitigate the adverse effects of unsymmetrical voltage-to-ground fault on the electric torque, stator, and rotor current transients, and the DC link voltage ripples of a wind-driven DFIG. In the first strategy, a STATCOM is connected to the stator terminals, while in the second proposed strategy a three-phase impedance is connected to the rotor circuit during fault conditions only. The third scheme involved both the STATCOM and added the rotor impedance. The performance of the DFIG under single-phase voltage sag is simulated for each scheme using Matlab/ Simulink. Simulation results for the three schemes are compared. The compared simulation results include the stator voltage and current, the rotor voltage and current, the dc-link voltage and current, the rotor speed, and the electrical torque. In addition, theoretical simulation results are compared for the sub and super-synchronous range of operation of the DFIG. It is well known that the current process for testing wind-driven generators under grid fault conditions is time and cost-intensive, as it requires the setup of the wind turbine and generator in the field. In addition, the complexity of the control algorithms and modelling of the overall DFIG system, especially during grid faults is another problem. Hence, a laboratory real-time simulator is essential for the test process. So, in this manuscript, a real-time simulator is employed to simulate a virtual DFIG subjected to an unsymmetrical grid voltage sag. The used real-time simulator is known as OPAL RT-4510. It is considered hardware-in-the-loop (HIL) and at the same time is a rapid control prototyping (RCP) platform. It is used for real-time emulation of the three protection schemes proposed to mitigate the electric torque oscillations, decrease rotor current transients, and decrease the DC link voltage ripples, resulting from unsymmetrical grid-voltage sag. The three systems models are then applied to the real-time simulator OPAL RT-4510 with down-sized signals compared with Matlab results. Emulation results are presented, showing good matching with the simulation results, hence proving the validity of the real-time emulator.

The contribution in this paper can be summarized as:

1- Using both STATCOM and external rotor impedance simultaneously for mitigating the effect of the unsymmetrical voltage sag.
2- Concluding the suitable protection scheme for the sub-synchronous speed range, which is found to be different from the suitable protection scheme for the super-synchronous speed range.
3- Emulation of the theoretical results, with exact matching, hence ensuring the feasibility of the results

The paper is organized as follows:
Section 1 is an introduction and the system description is explained in section 2. Section 3 implies the simulation tools with the HIL implementation. Simulation and real-time results for DFIG-operation at both sub- and super-synchronous speed are included in sections 4 and 5 respectively. Finally, the conclusion, and recommendations are included in section 6.

2 Description of the Proposed System

The DFIG, shown in Figure 1, is a three-phase wound-rotor induction machine whose stator windings are coupled to the power grid, while its rotor-windings are connected to the grid via two back to back converters. The wind-energy conversion systems (WECS) employing a DFIG are widely used as a variable-speed wind energy system. This is due to many advantages. One of these advantages is the easy control of the frequency and magnitude of the rotor current. Another advantage is its operation within wide range of rotor speeds, hence increasing the captured wind energy. The advantage, that makes the DFIG- based wind power system dominates, is that the rotor converters' rated power is only 30% of the generator’s rated power, so this method is advantageous from a cost perspective [28].

2.1 Wound Rotor Induction Machine Equations

The d-q axes equations describing the DFIG shown in Figure 1 are given as;

$$V_{ds} = R_s I_{ds} + p\lambda_{ds} - \omega\, \lambda_{qs} \quad (1)$$
$$V_{qs} = R_s I_{qs} + p\lambda_{qs} + \omega\, \lambda_{ds} \quad (2)$$
$$V_{dr} = R_r I_{dr} + p\lambda_{dr} - \omega_r \lambda_{qr} \quad (3)$$
$$V_{qr} = R_r I_{qr} + p\lambda_{qr} - \omega_r \lambda_{dr} \quad (4)$$
$$\lambda_{ds} = L_s I_{ds} + M I_{dr} \quad (5)$$
$$\lambda_{qs} = L_s\, I_{qs} + M\, I_{qr} \quad (6)$$
$$\lambda_{dr} = L_r\, I_{dr} + M\, I_{ds} \quad (7)$$
$$\lambda_{qr} = L_r\, I_{qr} + M\, I_{qs} \quad (8)$$

Electromagnetic torque equation:

$$T_e = 1.5\, P\, M\, (\lambda_{qs}\, I_{dr} - \lambda_{ds}\, I_{qr}) / L_s \quad (9)$$

Where suffixes s and r stand for stator and rotor parameters respectively, V is the voltage, I is current, λ is the flux, M is the mutual inductance, L is the self-inductance, R is the resistance per phase, ω is the synchronous speed, P number of pole pairs, and "p" is the d/dt operator.

2.2 Description of Fault Ride Through Systems

When the grid voltage drops, the active power generation decreases, leading to rapid rise in rotor current to compensate for the reduced active power. The high rotor current may exceed the converters' ratings, which result in tripping the WECS from the grid, leading to instability of the utility system.

To overcome this scenario Fault Ride Through (FRT) systems are imposed. The role of these systems is to sustain grid connectivity and inject reactive power during outages. A widely used technique for enabling FRT is FACTS devices. One of these devices that can generate or consume reactive power from the electric grid is a static-synchronous compensator (STATCOM). Another protection circuit proposed in the past literature is a crowbar circuit equipped with RL impedance in the rotor circuit. The crowbar allows a low resistance path during grid fault, thereby protects the rotor-side converter from over-currents. Hence the DFIG will start operating as a squirrel-cage induction machine, consuming reactive power, adversely affecting the grid voltage. To overcome the limitations caused by the crowbar, a simpler protection circuit, an R-L impedance is connected to the rotor circuit. This technique prevents the DFIG from acting as a squirrel cage induction machine. The FRT capability of these two systems are investigated and compared.

2.2.1 The DFIG with STATCOM

The STATCOM connection with the DFIG is shown in Figure 1, while its equivalent circuit is shown on Figure 2 connected to the point of common connection PCC. It consists of a two-level voltage source converter (VSC), a DC energy source (e.g. a capacitor), a passive filter, and a coupling transformer connecting the VSC in shunt with the distribution network. If the system voltage is less than the voltage at the STATCOM terminals, the STATCOM acts as a capacitor and reactive power is injected from the STATCOM to the system. On the other hand, if the system voltage is higher than the voltage at the STATCOM terminal, the STATCOM behaves as an inductor and the reactive power transfers from the system to the STATCOM. Under normal operating conditions, both voltages are equal and there is no power exchange between the STATCOM and the AC system. The differential equations for Figure 2 in three-phase form are, [27]:

$$\begin{aligned} \mathrm{L}\frac{\mathrm{di_a}}{\mathrm{dt}} &= -\mathrm{Ri_a} + (\mathrm{v_a} - v_{a1}) \\ \mathrm{L}\frac{\mathrm{di_b}}{\mathrm{dt}} &= -\mathrm{Ri_b} + (\mathrm{v_b} - v_{b1}) \\ \mathrm{L}\frac{\mathrm{di_c}}{\mathrm{dt}} &= -\mathrm{Ri_c} + (\mathrm{v_c} - v_{c1}) \end{aligned} \tag{10}$$

where i_a, i_b, i_c are the AC line currents of the STATCOM; v_a, v_b and v_c are the PCC voltages; υ_{a1}, υ_{b1} and υ_{c1} are the inverter terminal voltages; R and L represent the equivalent conduction losses and the transformer and filter. Inductance. The above equations are converted into a d-q synchronously rotating frame as:

$$\begin{aligned} L\frac{di_d}{dt} &= -Ri_d + \omega L i_q(v_d - v_{d1}) \\ L\frac{di_q}{dt} &= -Ri_q - \omega L i_d(v_q - v_{q1}) \end{aligned} \tag{11}$$

Where ω is the synchronous angular speed of the fundamental system voltage. Neglecting the inverter voltage harmonics, the voltage at the inverter output terminals are:

$$v_{d1} = Kmv_{dc}\sin\alpha$$
$$v_{q1} = Kmv_{dc}cos\alpha$$

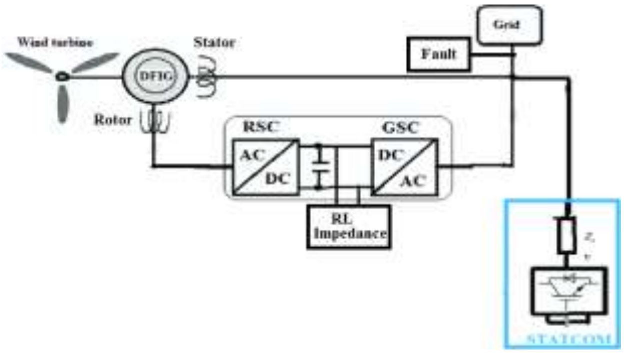

Fig. 1: Schematic diagram of a wind-driven grid-connected DFIG with STATCOM [1].

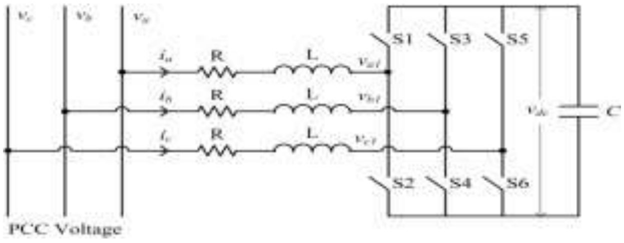

Fig. 2: The equivalent circuit of the STATCOM [1].

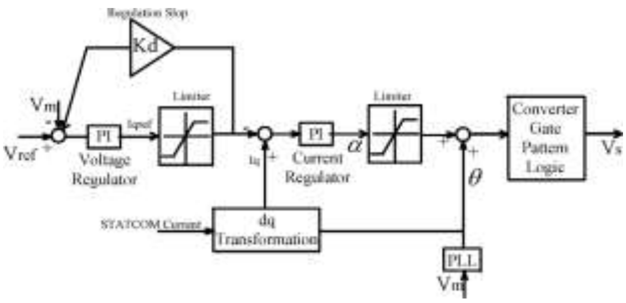

Fig. 3: STATCOM PI control block diagram [1].

Where K is the inverter constant, determined by the inverter structure, m is the modulation index of the PWM switching technique, υ_{dc} is the DC voltage across the STATCOM capacitor, and α is the inverter switching angle given as:

$$\begin{aligned} m &= \frac{\sqrt{v_{d1}^2+v_{q1}^2}}{Km} \\ \alpha &= \tan^{-1}\frac{v_{q1}}{v_{q1}} \end{aligned} \tag{12}$$

The instantaneous active and reactive power at the PCC is:

$$P = \frac{3}{2}\left(v_d i_d - v_q i_q\right)$$
$$Q = \frac{3}{2}\left(v_d i_d - v_q i_q\right) \quad (13)$$

The active and the reactive power exchange between the STATCOM and the AC system is controlled via the VSC firing angle "α" and the modulation index "m" to maintain the voltage at the point of connection and the DC-voltage within permissible limits. The system model given by the above equations, is used along with the PI controller to regulate the PCC voltage as shown in Figure 3, [4].

2.2.2 The DFIG with External Rotor Impedance

One of FRT methods in the literature is to install a crow bar together with a R-L impedance in series with the rotor windings of DFIG to limit both the stator and rotor currents. Since the crowbar activation causes the DFIG to consume reactive power, the FRT capability of a R-L impedance in series with the rotor windings, shown in Figure 4, is investigated. The rotor impedance consists of parallel R-L branch, which considerably reduces the rotor and stator over-current at the instants of grid faults occurrence. The proposed scheme decreases the electromagnetic torque oscillations and DC-link over-voltage.

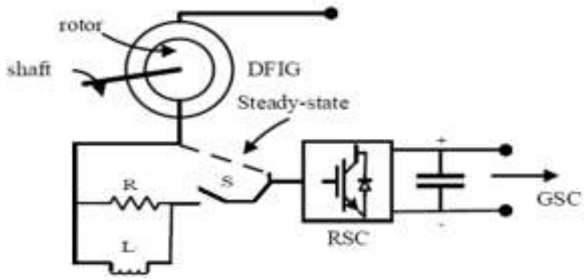

Fig. 4: DFIG with added RL rotor impedance [1].

3 Matlab/ Simulink Simulation and Real-Time Test

In the following sections, Matlab/Simulink results are presented and compared with real-time emulated results, showing reasonable matching, proving the validity of the proposed schemes. The data of the test machine is given in appendix a. Figure 5a show OP4510 block diagram, and Figure 5b is a photo of the experimental rig of the proposed system, Real-time digital hardware emulation technology is important in designing and testing most electrical schemes such as power systems, smart grids, motor drives, and power quality techniques. This technology saves time, protects real systems and operators from any dangerous effects, and introduces many test functionalities. This platform enables the user of the Matlab/ Simulink model to convert it to the real-time workshop and then download the real-time simulation into multicore multiprocessor hardware design. So, in this paper, one of the more efficient real-time simulators is used known as OPAL RT-4510. It is considered a hardware-in-the-loop (HIL) and at the same time is a rapid control prototyping (RCP) platform. This includes a Kintex-7 FPGA with Intel Xeon 4-core CPU processor, as shown in Figure 5a, [30]. In addition, it implies 32-channels for digital input/outputs and 16 analog channels. The output parameters for the proposed system are monitored through analog channels and measured as a real signal through a digital oscilloscope as illustrated in Figure 5b, [31]. The maximum output voltage signal for the analog channel is 16V, so, each output signal is scaled through the Simulink model according to its value. For example, the stator voltage and current waveforms are scaled down by 100 and 20 respectively. On the other hand, the rotor voltage and current waveforms are both scaled down by 50. But, torque and speed signals are scaled down by 50 and 20. Finally, the dc-link voltage and current waveforms are also scaled down by 20 and 5 respectively.

4 DFIG at Sub-Synchronous Speed

4.1 DFIG with STATCOM during Fault

A STATCOM is connected to the AC stator side. It consists of a voltage-controlled inverter fed via batteries and controlled by a proportional-integral (PI) controller to achieve automatic voltage regulation. A single-phase voltage to ground fault is assumed from time t= 0.5sec to 0.7 sec.

Figure 6a shows the Matlab/Simulink results of the stator voltage and current with STATCOM connected. The stator voltage and current restored their magnitude as the ground fault ended. Figure 6b presents the Real-time emulator results of the stator voltage and current with STATCOM connected, showing exact matching. Matlab/ Simulink results in Figure 7a shows a rise in the frequency of the rotor voltage and current during the fault, while their magnitudes are the same as in the normal operating condition. It is noted that sharp peaks occurred in the rotor current at the end of the fault. Figure 7b presents the Real-time emulator results of the rotor voltage and current, showing good matching.

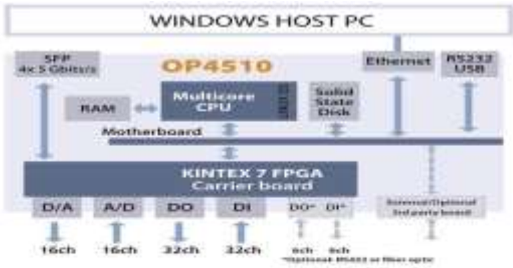

(a) OP4510 block diagram [30].

(b) Overall setup [31].

Fig. 5: Experimental rig for the proposed system.

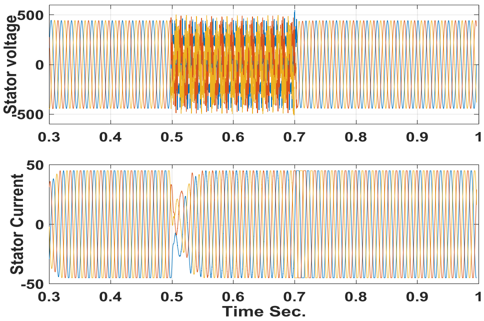

Fig. 6a: Simulation of stator voltage and current with STATCOM at sub-sync speed.

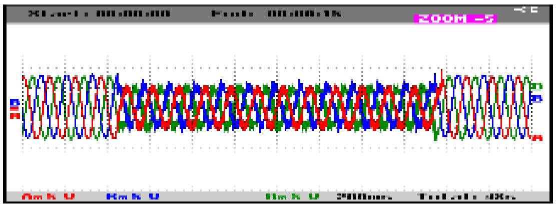

Stator voltage

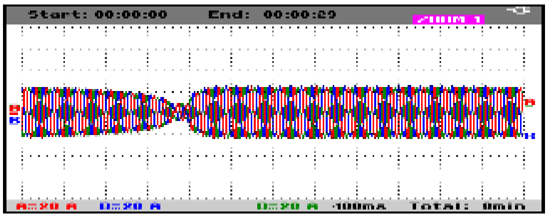

Stator current

Fig. 6b: Emulation of stator voltage and current with STATCOM during faults at sub-sync speed.

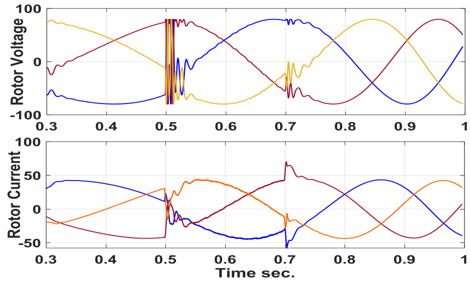

Fig. 7a: Simulation of rotor voltage and current with STATCOM during fault at sub-sync speed.

4.2 DFIG with Three-Phase Rotor Impedance

A three-phase RL impedance is added to the rotor circuit during the grid fault, with their values adjusted according to the machine rotor impedance to give optimum results. Figure 8a shows the simulation results of stator voltage and current, while Figure 8b presents the corresponding emulator results, with exact matching. The stable steady values of both components prove the validity of such a protection scheme. Figure 9a shows simulation results of the rotor voltage and current showing the complete cancellation of the effect of grid to ground fault, while Figure 9b shows the corresponding emulation results. However, Figure 10a showing the simulation results of the DC link voltage and current, reveal high peak in the current magnitude, and ripples in the DC voltage, while Figure 10b presents the matching corresponding emulation results. Hence additional protection method has to be added. Figure 11a shows the simulation results of rotor speed and electric torque respectively, with their emulation results shown in Figure 11b. Low ripples are presented in the torque during the single-phase fault, while a smooth speed profile is obtained.

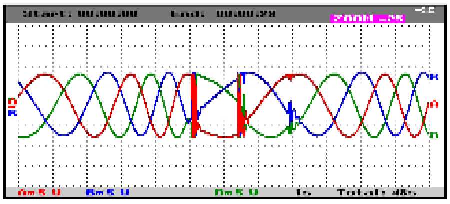

Rotor voltage

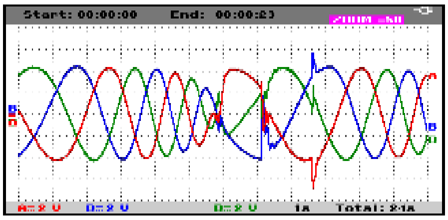

Rotor current

Fig. 7b: Emulation of rotor voltage and current with STATCOM during fault at sub-sync speed.

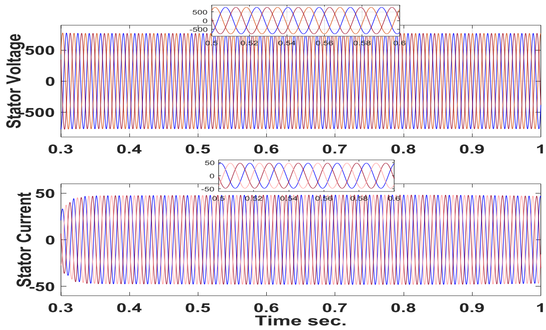

Fig. 8a: Simulation of stator voltage and current with three-phase RL impedance during faults.

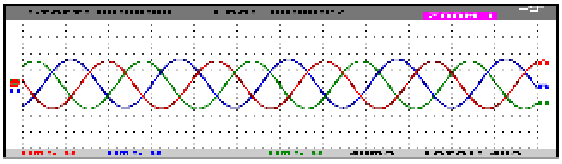

Stator voltage

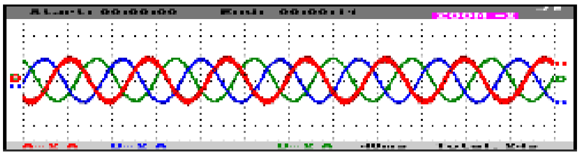

Stator current

Fig. 8b: Emulation of stator voltage and current with three-phase RL impedance during faults.

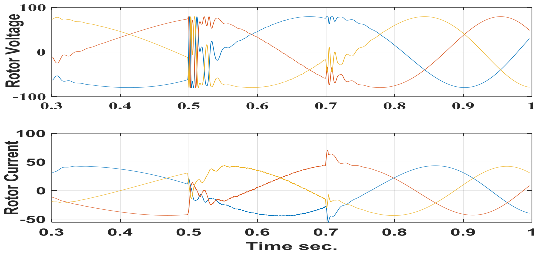

Fig. 9a: Simulation of rotor voltage and current with three-phase RL impedance during fault.

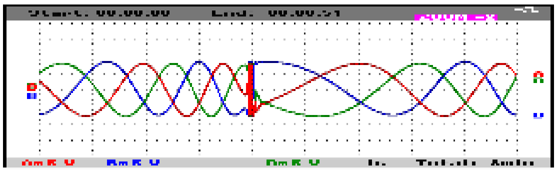

Rotor voltage

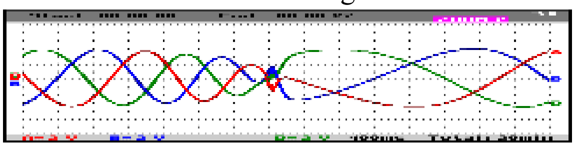

Rotor current

Fig. 9b: Emulation of rotor voltage and current with three-phase RL impedance during fault.

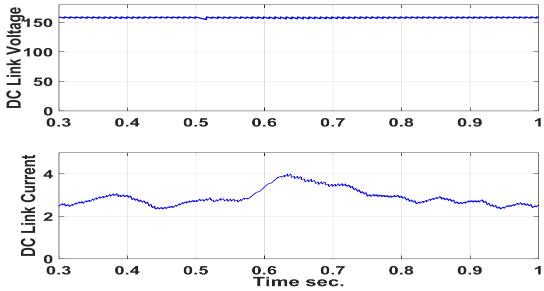

Fig. 10a: Simulation of DC link voltage and current with 3-phase RL impedance during fault.

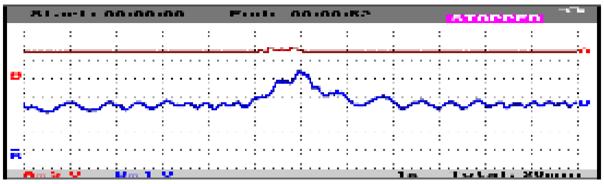

Ch. A (Voltage) Ch. B (Current)

Fig. 10b: Emulation of DC link voltage and current with 3-phase RL impedance during fault.

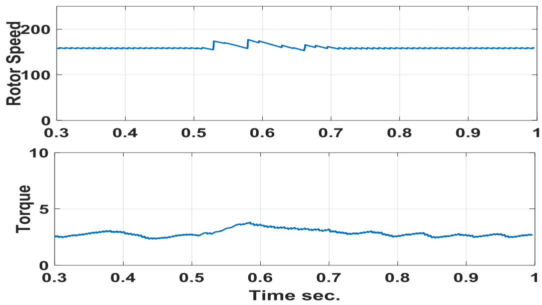

Fig. 11a: Simulation of rotor speed & electric torque with3-phase RL impedance during fault.

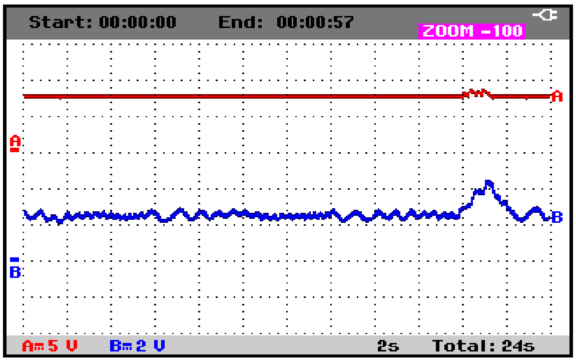

Ch. A (Speed) Ch. B (Torque)

Fig. 11b: Emulation of rotor speed & electric torque with3-phase RL impedance during fault.

4.3 DFIG with Three-Phase Rotor Impedance and STATCOM

The three-phase RL impedance is added to the rotor circuit during the grid fault in addition to the STATCOM device described previously. Figure 12a shows the Matlab/ Simulink results of rotor voltage and current showing the complete cancellation of the effect of grid to ground fault. Figure 12b shows the corresponding Real-time simulator results, where matching is clear. Figure 13a shows the Matlab/ Simulink DC link voltage and current, still containing a high peak in the DC current during the fault, and low ripples in the DC voltage. It is noted that the peak in the DC current is lower than that when applying the rotor impedance only. Figure 13b shows the emulation results of DC link voltage and current with clear matching. Figures 14a and Figure 14b show the Matlab rotor speed and electric torque and real-time simulation respectively, showing good matching. High torque peaks occurred at the beginning and the end of the ground fault.

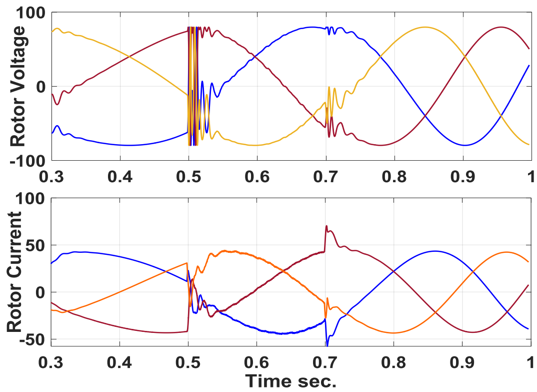

Fig. 12a: Matlab Rotor voltage and current with STATCOM and three-phase RL impedance during faults.

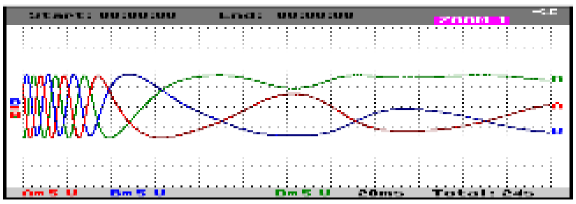

Rotor Voltage

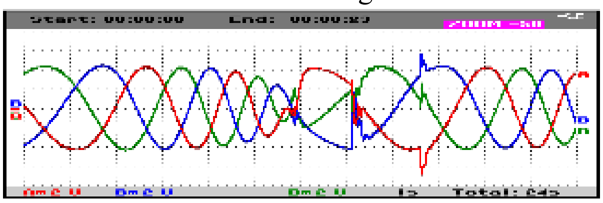

Rotor Current

Fig. 12b: Real-time simulation of Rotor voltage and current with STATCOM and three-phase RL impedance.

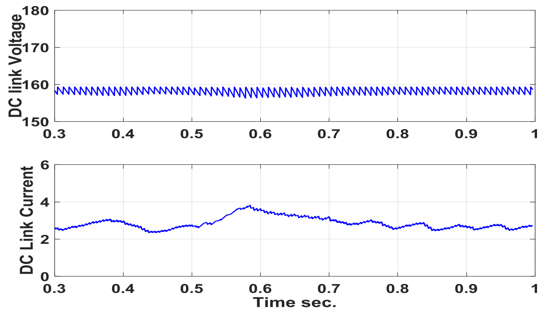

Fig. 13a: Matlab DC link voltage and current with STATCOM and three-phase RL impedance.

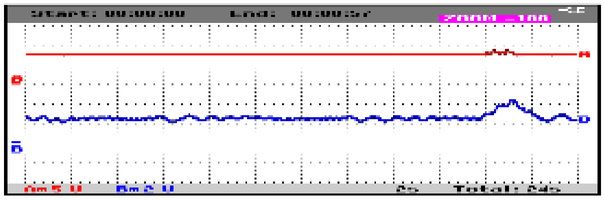

Ch. A (Voltage)Ch. B (Current)

Fig. 13b: Real-time simulation DC link voltage with STATCOM and three-phase RL impedance.

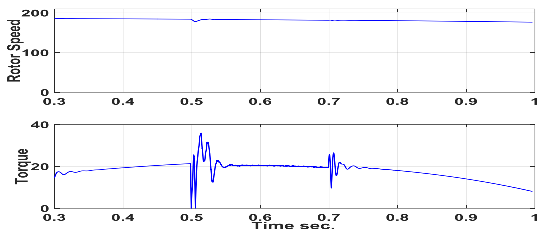

(a) Simulation Results

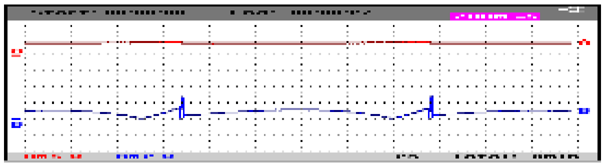

(b) RT-results: Ch. A (Speed) Ch. B (Torque)

Fig. 14a,b: Matlab and RT-Lab results for rotor speed and electric torque with STATCOM and three-phase RL impedance.

5 DFIG at Super-Synchronous Speed

5.1 DFIG with STATCOM during Fault

Figure 15a and Figure 15b show simulation and emulation results of stator voltage and current respectively. The magnitude of the stator current slightly increased than its steady-state value.

Figure 16a and Figure 16b present the simulation and emulation results of the DC link voltage and current. The figures show high ripples in the DC link voltage and low ripples in DC current. These current ripples lead to unstable electrical torque as shown in Figure 17a and Figure

17b. Hence using STATCOM as a protection method is not valid for mitigating the effect of unsymmetrical fault at the super-synchronous operation of the DFIG.

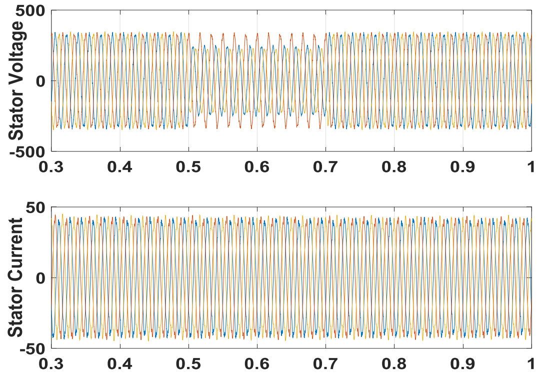

Fig. 15a: Simulation of stator voltage &current at super-sync speed with STATCOM.

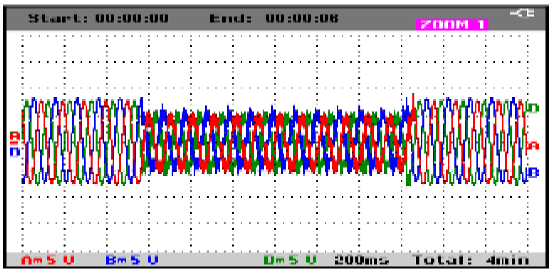

Stator voltage

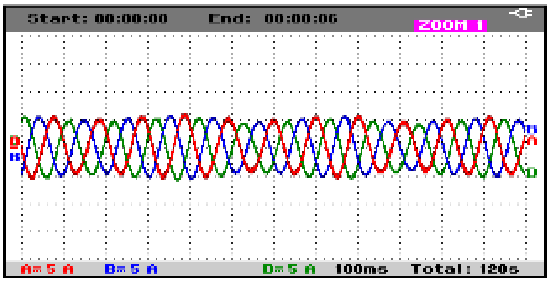

Stator current

Fig. 15b: RT results of stator voltage &current at super-sync speed with STATCOM.

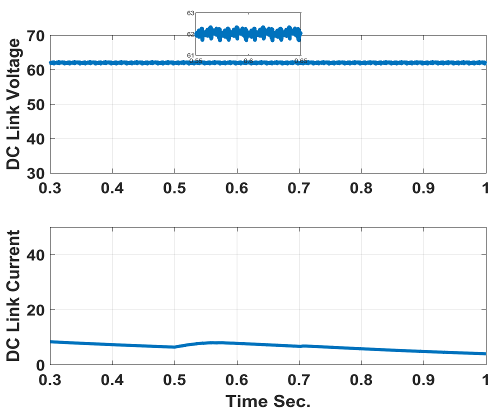

Fig. 16a: Simulation results of DC link voltage and current with STATCOM only during faults.

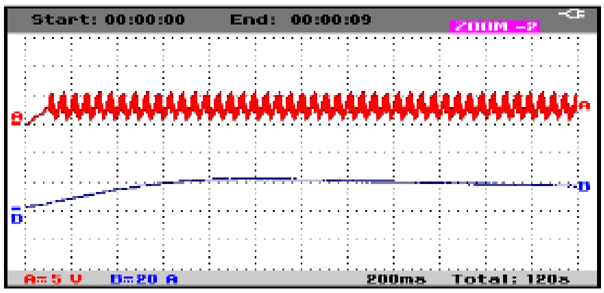

Ch. A (Voltage) Ch. B (Current)

Fig. 16b: RT results of DC link voltage and current at super-sync speed with STATCOM only during faults.

5.2 DFIG with External Rotor Impedance during Fault

Faster restoration of rotor voltage and current magnitudes are noticed than when using STATCOM as shown in Figure 18a and Figure 18b. However, considerable ripples are present in the rotor voltage. Consequently, the ripples in the DC current and DC voltage, as shown in Figure 19a and Figure 19b (simulation and emulation results) decreased than when using STATCOM only. Also, the ripples are low in the simulation and emulation results of electric torque and rotor speed shown in Figure 20a and Figure20b. Hence this protection method is effective for mitigating the unsymmetrical grid-to-ground fault at the super-synchronous range of operation of the DFIG.

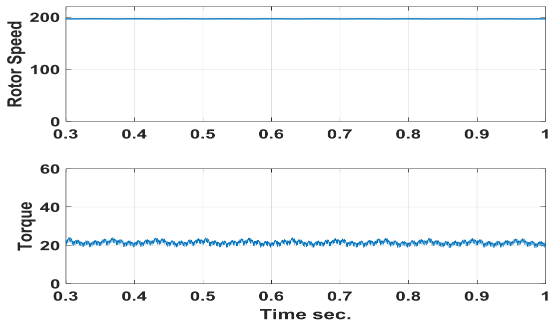

(a) Simulation

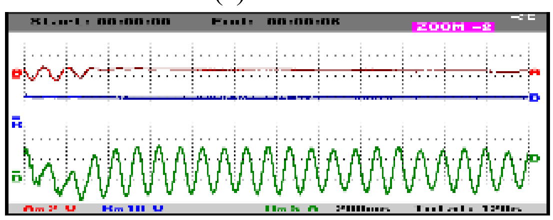

(b) Real-time

Fig. 17: Waveforms of speed and torque with STATCOM at super-synchronous speed..

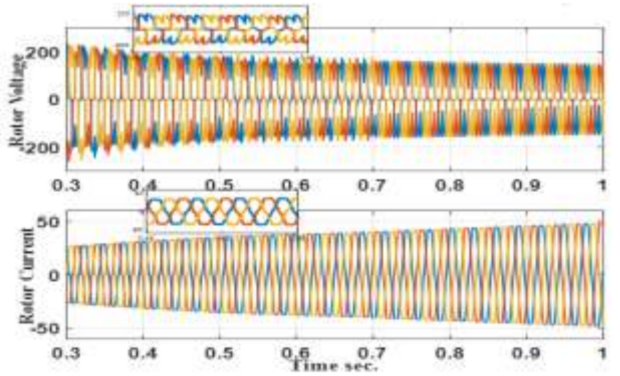

Fig. 18a: Simulation results of rotor voltage & current with 3-phase RL impedance at super-sync Speed.

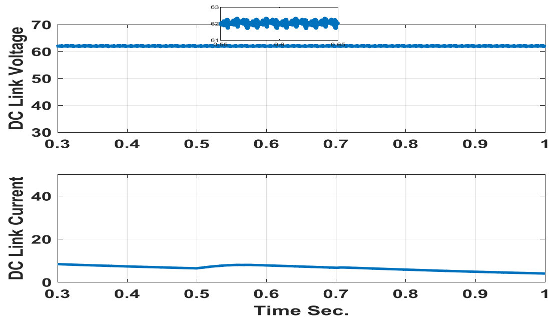

(a) Simulation

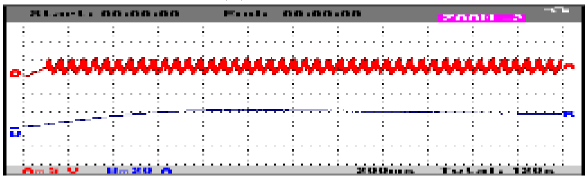

(b) Real-time: Ch. A (Voltage) and Ch. B (Current)

Fig. 19: DC-link voltage and current waveforms with 3-phase RL impedance at super-sync speed.

5.3 DFIG with Both STATCOM and External Rotor Impedance during Fault

The stator voltage and current restore their original values, as shown in Figure 21a and Figure 21b. However, the magnitude of the stator current fluctuates throughout the examined time, i.e. before and after the fault, as shown. The ripples in the DC current and DC voltage are shown in Figure 22a and Figure 22b are not reduced as in the scheme with STATCOM only which consequently affected the electrical torque shown in Figure 23a and Figure 23b. Hence, this protection scheme is not valid for mitigating the effect of unsymmetrical voltage to ground fault at super-synchronous speed range of operation.

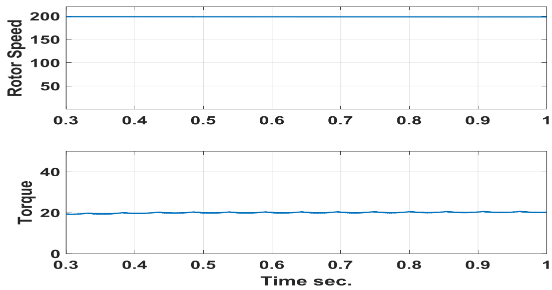

(a) Simulation

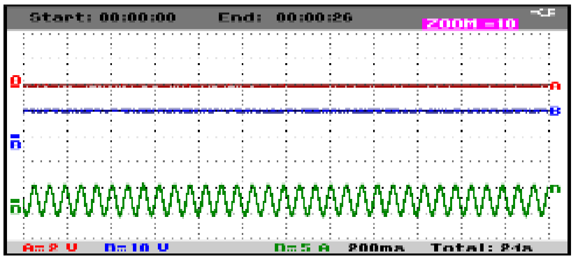

(b) Real-time: Ch. A (speed), Ch. B (torque), Ch. D (current)

Fig. 20: Rotor speed-torque waveforms with three-phase RL impedance at super-sync speed.

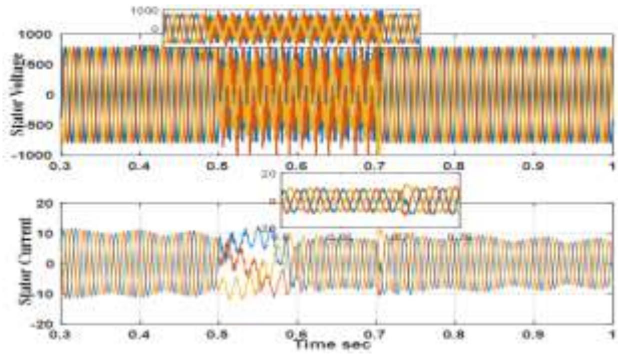

Fig. 21a: Simulation of stator voltage & current with STATCOM &rotor impedance at super-sync speed.

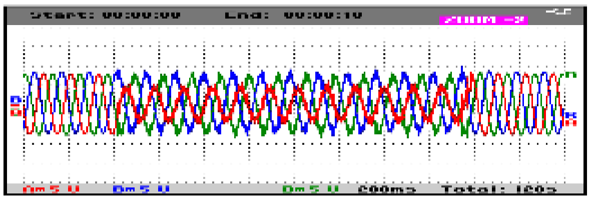

Stator Voltage

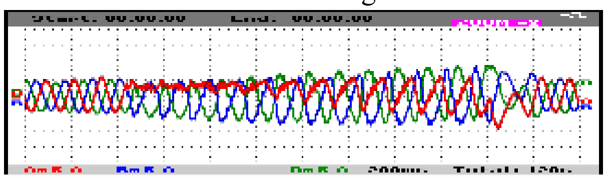

Stator Current

Fig. 21b: Emulation of stator voltage & current with STATCOM &rotor impedance at super-sync speed.

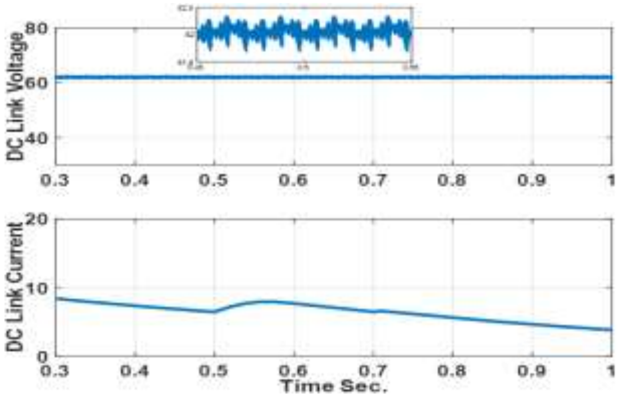

(a) Simulation

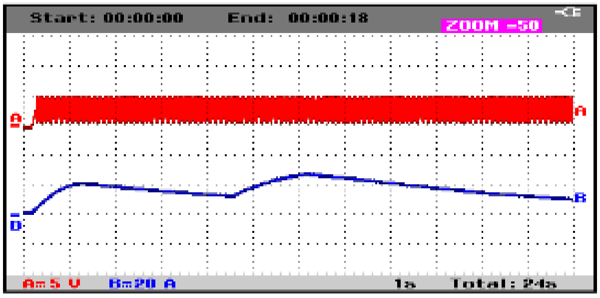

(b) Real-time: Ch. A (Voltage), Ch. B (Current)

Fig. 22: DC-link voltage and current with STATCOM and 3-phase rotor impedance at super-synchronous speed.

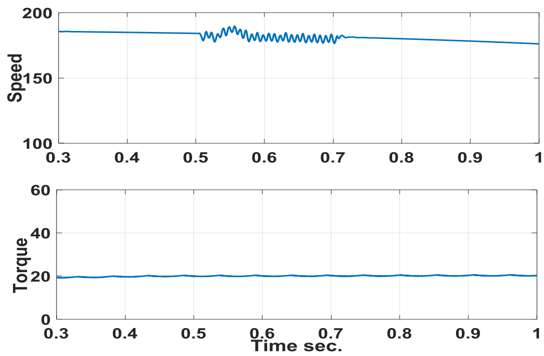

(a) Simulation

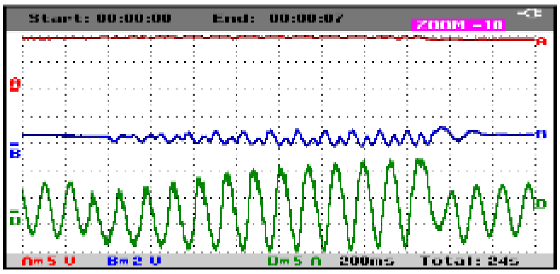

(b) Real-time: Ch. A (Speed), Ch. B (Torque), Ch. D (current)

Fig. 23: Results of rotor speed and torque with STATCOM and 3-phase RL impedance at super-synchronous speed.

6 Conclusion

In this paper, three fault-ride-through schemes are proposed to mitigate the effect of unsymmetrical voltage to ground fault on a grid-connected DFIG coupled to a wind turbine. The first scheme comprises a STATCOM connected to the DFIG stator, while a three-phase external impedance is connected to the rotor circuit in the second scheme. The third scheme comprised both the STATCOM and the rotor impedance. Matlab/ Simulink simulation results of the stator and rotor voltages and currents, the dc-link voltage and current, the electrical torque, and the rotor speed are presented at sub-and super-synchronous speeds for the three proposed schemes. All systems were emulated, implemented, and tested through an OPAL RT-4510 Digital Real-Time Simulator (DRTS) in a Hardware-In-the-Loop (HIL) application. All real-time waveforms of parameters for the proposed scenarios were monitored through the HIL-controller and data acquisition interface and then compared with the simulated results. The results reveal that both are congruent. The unsymmetrical ground fault effect on the DFIG voltages, currents, electrical torque, and speed is mitigated when using both devices at the sub-synchronous range of operation. While, the unsymmetrical ground fault effect on the DFIG voltages, currents, electrical torque, and speed is mitigated when using the external rotor impedance only at super-synchronous speed.

APPENDIX A

The main data of the test DFIG is:
S=3.7 KVA, V_S=460V, f =60 Hz, $R_S = 1.115\ \Omega$, R_r=1.083Ω, $L_S = L_r = .005974$ H, L_m=0.203 H
J=0.02 Kg.m², B=0.005752 N.m.s.

References:

[1] M. Eskander, M. Saleh, M. El-Hagry, “Performance of Double Fed Induction Machine at Sub- and Super- Synchronous Speed in Wind Energy Conversion System”, *Journal of Power Electronics*, JPE 9-4-7, 2009, pp. 575-58.

[2] Yun Wang, Qiuwei Wu, Honghua Xu, Qinglai Guo, and Hongbin Sun., “Fast Coordinated Control of DFIG Wind Turbine Generators for Low and High Voltage Ride-Through”, *Energies* 2014, *7*, 4140-4156.

[3] M. N. Eskander, M.A.Saleh, Maged N.F.Nashed, S. Amer., “Superiority of LVRT

of Grid Connected Wind Energy Conversion System Using Unified Power Quality Controller", *International Electrical Engineering Journal*, Vol. 6, no.6, 2015, pp. 1925-1930.

[4] G. Parameswari and H. Sait, "A comprehensive review of fault ride-through capability of wind turbines with a grid-connected doubly fed induction generator", *Int. Trans. Elec. Energy Syst.*, Vol. 30, no. 8, 2020, pp. 1–30, https://doi.org/10.1002/2050-7038.12395.

[5] A. Rola´n, F. Co´rcoles, J. Pedra, "Behavior of the doubly-fed induction generator exposed to unsymmetrical voltage sags", *IET Electrical Power Applications*, Vol. 6, no. 8, 2012, pp. 561–574.

[6] W. Zaijun, Z. Chanxia and H. Minqiang, " Improved Control Strategy for DFIG Wind Turbines for Low Voltage Ride Through, *Energies*, Vol. 6, 2013, pp. 1181-1197; https://doi:10.3390/en6031181.

[7] H. Mohammadpour, S. G. Zadeh, S. T., "Symmetrical and asymmetrical low-voltage ride-through of doubly-fed induction generator wind turbines using gate-controlled series capacitor", *IET Renewable Power Generation,* 2015, pp1-7.

[8] Donghai Zhu; Xudong Zou; Lu Deng; Qingjun Huang; Shiying Zhou; Yong Kang, "Inductance emulating control for DFIG-based wind turbine to ride-through grid faults", *IEEE Trans. Power Elect*., Vol. 32, no. 11, 2017, pp. 8514–8525.

[9] Donghai Zhu; Xudong Zou; Shiying Zhou; Wen Dong; Yong Kang; Jiabing Hu, , "Feed-forward current references control for DFIG-based wind turbine to improve transient control performance during grid faults", *IEEE Trans. Energy Conversion*, Vol. 33, no. 2, 2018, pp. 670–681.

[10] A. Falehi and M. Rafiee, "LVRT/HVRT capability enhancement of DFIG wind turbine using optimal design and control of novel PIλDμAMLI based DVR", *Sustain. Energy, Grids and Network,* Vol. 16, 2018, pp. 111–125, https://doi.org/10.1016/j.segan.2018.06.001

[11] M. Morshed and A. Fekih, "A Fractional Order SMC approach to Improve the Reliability of Wind Energy Systems During Grid Faults", *IFAC-Papers On Line*, Volume 53, Issue 2, 2020, Pages 12109-12114.

[12] Z. Zou, J.Liao, Y.Lei, Z.Mu, X.Xiao, "Post-fault LVRT performance enhancement of DFIG using a stage-controlled SSFCL-RSDR", *IEEE Trans. On Applied. Superconductivity*, Vol. 29, no. 2, 2019.

[13] O. M. Kamel, A. Diab, T. Do, and M. Mossa, "A novel hybrid ant colony-particle swarm optimization techniques based tuning STATCOM for grid code compliance", *IEEE Access*, Vol. 8, 2020, pp. 41566–41587.

[14] I. Khan, K. Zeb, W. Ud Din , S. Islam , M. Ishfaq, S. Hussain and H. Kim., "Dynamic Modelling and Robust Controllers Design for Doubly Fed Induction Generator-Based Wind Turbines under Unbalanced Grid Fault Conditions, *Energies*, Vol. 12, 2019.

[15] D. Sun, , Y. Wang , T. Jiang , X. Wang , J. Sun and H. Nian "Multi-Target Control Strategy of DFIG Using Virtual Synchronous Generator Based on Extended Power Resonance Control under Unbalanced Power Grid", *Energies*, Vol. 13, 2020.

[16] M. Liu, W. Pan, Y. Rao, C. Li, T. Liu, Z. Zhu, Y. Zhang, "An electromagnetic transient analysis model for DFIG considering LVRT hardware protection", *IEEE Access*, Vol. 9, 2021, pp. 32591–32598.

[17] J. Nikolaos; E. Tsioumas; C. Mademlis; E. Solomin, "Highly Effective Fault-Ride-Through Strategy for a Wind Energy Conversion System With a Doubly Fed Induction Generator", *IEEE Trans. on Power Electronics*, Vol. 35, no. 8, 2020, pp.8154-8165.

[18] P. Tripathi, S. Sahoo, and K. Chatterjee, "Enhancing the fault ride-through capability of DFIG-based wind energy system using saturated core fault current limiter", *IET Journal of engineering (Joe)*, 2019, Vol. 18, pp. 4916–4921.

[19] J. Guo; Ke Ren; X. Yang; J. Si; P. Yue; R. Khan, "Improved park inverse transform algorithm for positive and negative sequence separation of grid voltage under unbalanced grid conditions, *Proceeding of Chinese Control Conf.*, 27-30 July 2019, Guangzhou, China, pp. 7256–7262.

[20] V. Suppioni, A. Grilo, and J. Teixeira, "Coordinated control for the series grid side converter-based DFIG at sub-synchronous operation, *Electric Power System Research*, Vol. 173, 2019, pp. 18-28.

[21] J. Huang and S. Li, "Asymmetrical LVRT of DFIG incorporating feed-forward transient current control and controllable resistive-type fault current limiter", *IEEJ Trans. Electrical*

and Electronic Eng., Vol. 15, no. 7, 2020, pp. 1100-1108.

[22] Z. Rafiee, S. S. Najafi, M. Rafiee, M. R. Aghamohammadi, M. Pourgholi., “Optimized control of coordinated series resistive limiter and SMES for improving LVRT using TVC in DFIG-based wind farm”, *Physica C: Superconductivity and its Appl.*, Vol. 570, 2020.

[23] Waqar Uddin, Kamran Zeb, Ayesha Tanoli, Aun Haider, “Hardware-based hybrid scheme to improve the fault ride-through capability of doubly fed induction generator under symmetrical and asymmetrical fault”, *IET Generation, Transmission and Distribution*, Vol. 12, no. 1, 2018, pp. 200-206.

[24] J. Sun, J. Yi, and Z. Pu, “Fixed-time adaptive fuzzy control for uncertain non-strict-feedback systems with time-varying constraints and input saturation”, *IEEE Trans. Fuzzy Syst.*, Vol. 29, Iss. 12, 2021, pp. 3769 – 3781.

[25] N. Hannoon, D. V. N. Ananth, Bin Hidayat, P. S. R. Chowdary, V. Chakravarthy, K. SivashankarI, and S. Satapathy “A Common Capacitor Based Three Level STATCOM and Design of DFIG Converter for a Zero-Voltage Fault Ride-Through Capability”, *IEEE Access*, Vol. 9, 2020, *pp.* 105153- 105179.

[26] M. Ahmed, T. Kandil, and E. Ahmed, “Enhancing Doubly Fed Induction Generator Low-Voltage Ride-through Capability Using Dynamic Voltage Restorer with Adaptive Noise Cancellation Technique”, *Sustainability*, Vol. 14, no 2, 2022, 859.

[27] Ahsan Iqbal, Ayesha Ayoub , Asad Waqar , Azhar Ul-Haq , Muhammad Zahid, and Syed Haider., ”Voltage stability enhancement in grid-connected microgrid using enhanced dynamic voltage restorer (EDVR)”, *AIMS Energy*, Vol. 9, no. 1, 2021, pp. 150-177, https://doi:10.3934/energy.2021009.

[28] Md Nafiz Musarrat, Afef Fekih, and Md Rabiul Islam, " An Improved Fault Ride Through Scheme and Control Strategy for DFIG-Based Wind Energy Systems", *IEEE Trans. on Applied Superconductivity*, Vol. 31, No. 8, Nov. 2021.

[29] Zhongliang Li, Fang Liu, " Frequency and voltage regulation control strategy of Wind Turbine based on supercapacitors under power grid fault", Energy Reports, Vol.10, pp.2612–2622, 2023

[30] Opal Co., “OP4512 Compact Entry-Level RCP-HIL FPGA-Based Real-Time Simulator”, *User’s Manual*, March 2023, Montréal, Québec, Canada.

[31] Opal Co., “OP8660 HIL Controller and Data Acquisition Interface”, *User’s Manual*, October 2023, Montréal, Québec, Canada.

Contribution of Individual Authors to the Creation of a Scientific Article (Ghostwriting Policy)

- Essamudin Ali Ebrahim has written and implemented of the part Real Time. He organized and executed the experimental work with paper revision.
- Maged N. F. Nashed has carried out the simulation.
- Mona Eskander was the one who presented the idea and wrote the article.

Sources of Funding for Research Presented in a Scientific Article or Scientific Article Itself

No funding was received for conducting this study.

Conflict of Interest

The authors have no conflicts of interest to declare.